Mesoscale cortical calcium imaging reveals widespread synchronized infraslow activity during social touch in mice.

Federico Bolaños[1,2,], Luis A. Bolaños[1,2,], Matilde Balbi[1,2,], Nicholas J. Michelson[1,2,], Jeffrey M. LeDue[1,2,], and Timothy H. Murphy[1,2,]

[1]Department of Psychiatry, Kinsmen Laboratory of Neurological Research; [2] Djavad Mowafaghian Centre for Brain Health, University of British Columbia, Vancouver, British Columbia, Canada, V6T 1Z3

Address: 2255 Wesbrook Mall, Detwiller Pavilion, Vancouver, B.C. V6T 1Z3, Canada

E-mail: thmurphy@mail.ubc.ca, federico.bolanos@riken.jp

Acknowledgements: This work was supported by a Canadian Institutes of Health Research (CIHR) T.H.M FDN-143209 and from Brain Canada for the Canadian Neurophotonics Platform to THM and the Brain Canada Multi-Investigator Research Initiative program that THM was part of. CIHR or Brain Canada had no involvement in the research or decision to publish. We thank Pumin Wang for help with surgery and Matthieu P. Vanni, Allen W. Chan, Dongsheng Xiao and Alexander McGirr for helpful discussion and comments.

Contributions: F.B., L.B., M.B., N.J.M., and T.H.M. performed animal experiments. F.B., T.H.M., and J.M.L.wrote the paper. F.B., L.B., J.M.L., and T.H.M. developed the hardware and software for the apparatus. F.B. and J.M.L wrote the analysis. L.B., F.B., and J.M.L drew models and figures.

Competing financial interests: The authors declare no competing financial interests.

***Correspondence to:** Timothy H Murphy and Federico Bolanos

Abstract

We employ cortical mesoscale GCaMP6s imaging of intracellular calcium levels to establish how brain activity is correlated when two mice engage in a staged social touch-like interaction. Using a rail system, two head-fixed mice begin at a distance where social touch is not possible (160 mm), after 90s they are brought so that macrovibrissae contact each other (6-12 mm snout to snout) for an additional 135s. During the period before, during, and after contact cortical mesoscale GCAMP6 signals were recorded from both mice simultaneously. When the mice were together we observed bouts of mutual whisking resulting in cross-mouse correlated barrel cortex activity. While correlations between whisker cortices were expected given mutual whisking, we also found significant synchronized brain-wide calcium signals at a frequency band of 0.01-0.1Hz when the mice were together. We present dual mouse brain imaging as new paradigm to assess social interactions in a more constrained manner. The effects of social interaction extend outside of regions associated with mutual touch and have global synchronizing effects on cortical activity.

Keywords: mouse, cortex, social interaction, GCAMP, mesoscale, whisker

Introduction:

The power of social interaction and touch is undisputed across the animal kingdom. To evaluate neuro-correlates of social behavior, recent studies have focused both on systems level human work (Funane et al., 2011; Liu et al., 2017; Montague et al., 2002) to mechanistic studies within animal models (Gunaydin et al., 2014). Mechanistic studies on interactions between rodents indicate a fundamental role of the rodent vibrissal system in transmitting social signals (Bobrov et al., 2014; Ebbesen et al., 2017; Lenschow and Brecht, 2015). Mice use their highly sensitive vibrissae (whiskers) to locate objects (O'Connor et al., 2010), discriminate textures (J. L. Chen et al., 2013), and interact with other mice (Brecht and Freiwald, 2012; Grant and Mackintosh, 1963). Whiskers can be subdivided into two types; the micro and macrovibrissae (Deschênes et al., 2012). The longer macrovibrissae are closely linked with sniffing and are swept forward (protracted) to provide tactile feedback (Deschênes et al., 2012) during face to face social interactions (Ebbesen et al., 2017).

Mice, like other rodents, display a multitude of social behaviors, most of which can be classified into four categories: attending, approaching, investigating and nosing (Grant and Mackintosh, 1963). Recently, head-fixed rats have been used to elucidate a cortical signature of facial social interaction using electrophysiological read-out with micro/nanostimulation and pharmacological interventions (Bobrov et al., 2014; Ebbesen et al., 2017; Lenschow and Brecht, 2015). Rat social touch was associated with large membrane potential changes and depolarizations that were locked to the rat's whisking (Lenschow and Brecht, 2015). While these studies were elegant, they were restricted to barrel cortex electrophysiological recordings. Mice engage in a similar behavior wherein close proximity to another mouse triggers directed vibrissae movement (Grant and Mackintosh, 1963). However, in mice the cortical activated signature of this behavior remains unknown. While considerable work has been done in both human (Funane et al., 2011; Montague et al., 2002) and animal models (Gunaydin et al., 2014) regarding imaging or

photometric studies of between brain interactions, correlations between subjects over relatively high sampling rates and large expanses of cortex have not been established. We present a new paradigm where staged interactions between mice occur during simultaneous multi-subject cortical functional imaging using GCaMP to resolve cortical networks at the mesoscale level of organization (Allen et al., 2017; Gilad et al., 2018; Ma et al., 2016b; Murphy et al., 2016; Stringer et al., 2018; Vanni and Murphy, 2014; Zhuang et al., 2017). We find that face to face interactions between mice synchronize cortical activity over wide-scales and this phenomenon is not limited to regions primarily processing whisker touch-dependent signals.

Methods

Animals

All procedures were approved by the University of British Columbia Animal Care Committee and conformed to the Canadian Council on Animal Care and Use guidelines and reported according to the ARRIVE guidelines. Transgenic GCaMP6 mice C57BL/6J-Tg(Thy1-GCaMP6s)GP4.3Dkim/J (Dana et al., 2014) or tetO-GCaMP6s x CAMK tTA (Wekselblatt et al., 2016) were obtained from the Jackson Laboratory. The Thy1-GCaMP6 mouse line expresses GCaMP6s in layers 2/3 of the cortex, and the Thy1 promoter leads to expression predominantly in excitatory neurons (Dana et al., 2014). We used three cages of adult male mice (all greater than 60 days of age): one cage of four litter-mates, another cage of two litter-mates (both Thy1-GCAMP6), and a third cage of 2 pooled males (tetO-GCaMP6s x CAMK tTA); however, only three mice from the cage of four were usable because one of the chronic windows was of poor quality for imaging.

Chronic Window Surgery

Chronic windows were implanted on male mice that were at least 8 weeks old, as previously described in (Silasi et al., 2016). Briefly, we remove the fur and skin from the dorsal area of the head exposing the skull and fix a custom-cut coverslip and attachment bar (Figure 1). The area exposed includes the entire two dorsal brain hemispheres and the temporalis muscle at the back of the cranium (Figure 1A,B). Using super glue, a titanium bar (Figure 1D), which is used during head fixing, is attached to the posterior part of the skull with the top edge of the bar resting above lambda and is then reinforced with clear dental cement (Metabond). To attach the bar the skull is cleaned with phosphate buffered saline solution and a small drop of very diluted dental cement is added. We overlay a custom cut coverslip on top of the skull, gluing it with the dental cement, with the edges of the window then reinforced with a thicker mix of the dental cement (Figure 1A,C) similar to the procedure of (Silasi et al., 2016). The mice are then allowed to recover for at least seven days prior to any imaging.

Social Touch Experiments

Our goal was to have mice engage in a social touch like interaction, a behavior that was similar to the one previous rat experiments have developed (Bobrov et al., 2014; Ebbesen et al., 2017; Lenschow and Brecht, 2015). However, our aim was to image the entire dorsal surface of the cortices of both of the interacting mice simultaneously and not require investigator handling during the social presentation. To achieve this goal we built two Raspberry Pi-based imaging rigs that were placed facing each other, and henceforth we refer to the mouse on the left rig as the left mouse and the mouse on the right rig as the right mouse. The right mouse's rig was placed on top of a (translatable) rail (Edmunds Optics #56-798) so we could vary the distance between the snouts of the mice while continuously imaging both animals (Figure 1E). The distance between the snouts of the mice was changed between a maximum of 160mm (no social touch), to a minimum of 6-12mm (social touch possible) (Figure 1A). By bringing the mice to 6-12mm between each other (while imaging), the mice would engage in a social touch like behavior, in a

similar fashion Lenschow and Brecht 2015 using rats (Lenschow and Brecht, 2015). This procedure resulted in two types of experiments: 1) together experiments and 2) separate experiments.

Mice Together Experiments

In this type of experiment, we imaged the brain activity of each mouse for five min and 50 s. The mice started at distance of 160mm, and they stayed at this point for 90 s. At the 90 s mark we began decreasing the distance between the mice at a rate of ~9mm/s, by the 105 s mark the distance between the mice was 6-12mm. The mice were then kept at this distance for 135 s and at 240 s the distance between the mice was increased at a rate of ~9mm/s. By the 255 s the snouts of the mice were back at the initial 160mm. The distance remained at 160mm until the end of the experiment at the 5:50 min mark. A third camera, equipped with infrared lights, was positioned to record the behavioral activity of each mouse while they were together .

Mice Separate Experiments

In this type of experiment, we imaged the mice for 5:50 min/s. The difference between the together experiments and the separate experiments is that in the separate experiments the distance was never changed. So the mice were imaged at a constant distance of 160mm for the entire 5:50 min/s duration of the experiment. For this type of experiment the behavioral camera only had a view of the left mouse throughout the imaging session.

Sequence of Experiments

Each pair of mice was subjected to both types of experiments in the same session. For example, a pair of mice would be head-fixed and we would begin with the separate experiment first and then after that experiment is over we immediately start the together experiment, on one occasion the two types of

experiments were performed on separate days for a pair of mice. The order of separate vs together experiments would be chosen at random to avoid having some order dependent effect. If a mouse was to be head-fixed again for another pair we would give that mouse a half an hour break before head-fixing the mouse again, this was done to avoid any effect of being head-fixed for long periods of time.

Image Acquisition

Mesoscale GCaMP Imaging

GCaMP activity in the left and right mice was imaged using Raspberry Pi Cameras (OV5647 CMOS chip) equipped with a triple-bandpass filter (Chroma 69013m). The lens on the camera has a focal length of 3.6mm and was focused at a height that gave a field of view of 8mm x 8mm leading to a pixel size of 31.25 microns. RAW RGB (24-bit 256x256 resolution) images of GCaMP activity were captured at a frame rate of 28.815Hz, using a custom-written Python software on the Raspberry Pi single board computer. An additional Raspberry Pi Camera, the NOIR version (infrared filter not present) was placed between the mice to record their behavior (see next paragraph for details). The three cameras (2 brain and 1 behavior) were arranged in a master-slave mode, wherein one camera (master) was used to start the acquisition of the other two cameras (slaves). Each cortex was illuminated using 2 light emitting diodes (LEDs) simultaneously (launched into a liquid light guide), where one light source (short blue, 447 nm with Thorlabs FB 440-10 nm band pass filter) provides information about the hemodynamic changes during the experiment (Xiao et al., 2017), and the other light source (long blue, 473 nm with Chroma 480/30 nm) excites GCaMP. The excitation lights were turned on and off simultaneously using a master transistor-transistor logic output from an isolated pulse stimulator (AM-Systems) which was manually triggered immediately after the start of each experiment. This sudden change in illumination was used during post-hoc analysis to synchronize frames on each brain imaging and behavioral camera.

Behavior Imaging

The experimental setup was illuminated with two infrared (850 nm) LEDs, which allowed for the recording of behavioral activity without affecting the GCaMP imaging. Behavioral video was captured using the same OV5647 CMOS chip but, with an infrared version of the camera. H.264 encoded video was captured at a framerate of 90Hz with a resolution of 320x180 pixels. The camera was positioned such that both mice were clearly visible during together experiments while the right mouse was presented to the left mouse. At the beginning and end of the together experiments where the mice were separated, the field of view included only the left mouse.

Image Processing

Mesoscale GCaMP Imaging

The two RAW RGB 24-bit videos of calcium activity for each mouse were imported using the numpy Python library on a Jupyter Notebook (Kluyver et al., 2016). We extract the green and blue channel, which contain the green GCaMP6s fluorescence and the blood volume reflectance signals, respectively. With the current recording setup, the Raspberry Pi cameras occasionally drop frames as a result of writing the data to the disk. However, we quantified the exact number and location of dropped frames by tagging each frame with a timestamp, and found that the system generally dropped <0.01% of frames. Given the small number of dropped frames, and the relatively slow kinetics of GCaMP6s (T.-W. Chen et al., 2013), the lost data was estimated by interpolating the signal from each pixel.

The baseline image, or the mean across time for the entire recording, was subtracted from each individual frame (ΔF). This difference was then divided by the baseline, yielding the fractional change in intensity for each pixel as a function of time ($\Delta F/F_0$). The $\Delta F/F_0$ signal was then temporally filtered using a 3rd

order Chebyshev Type I bandpass filter with a low frequency cut-off of 0.01Hz and a high frequency cut-off of 12.0Hz, as most of the information of GCaMP6s can be captured in this band (Vanni and Murphy, 2014).

Mesoscale Reflectance Imaging

GCaMP green epifluorescence and long blue excitation light are both absorbed to a different degree, depending on the proportion of oxygenated and deoxygenated hemoglobin in that area of the brain (Ma et al., 2016a) (Wekselblatt et al., 2016). Therefore, the readout epifluorescence signal will be influenced by hemodynamic activity. For example, neural activity elicits localized increases in blood flow within the surrounding tissue, resulting in increased absorbance of light at both epifluorescence (520 nm) and excitation (473 nm) wavelengths. We try to estimate the contribution of these hemodynamic variations by also imaging with a short blue reflectance light channel. We chose the peak wavelength of 440 nm because it is close to an isobestic point, where the difference in absorbance by oxygenated hemoglobin and deoxygenated hemoglobin are negligible. Additionally, this wavelength falls within the blue band of the RGB camera sensor, allowing for simultaneous acquisition of fluorescence and reflectance data. Note the 440 nm reflectance light used for reference imaging is relatively dim (compared to 473 nm excitation) and does not contribute to green epifluorescence signal measured in the green channel of the RGB sensor using the 480/30 nm filter. To decrease the contribution of the hemodynamics to the epi-fluorescence signal we used a method that has been described in a previous paper from our laboratory (Xiao et al., 2017). In this previous work (Xiao et al., 2017) we validate the method by showing that the short blue reflected light signal correlates well with a green reflected light signal commonly used in a similar corrective strategy (Wekselblatt et al., 2016). Briefly, we divide the $\Delta F/F_{0GCaMP}$ (fluorescence) by $1+\Delta F/F_{0Blue}$ (1 + reflectance). In this way, small changes (near 0) in the blue reflectance signal do not influence the epifluorescence signal. This works well enough due to the fact that the hemodynamic

changes are relatively small compared to the signal-to-noise ratio (SNR) of signal of GCaMP6 (Dana et al., 2014; Ma et al., 2016a). While we acknowledge that a multi-wavelength and green reflectance strobing and model-based correction may be advantageous (Dana et al., 2014; Ma et al., 2016a), certain technical aspects of the Raspberry Pi camera (which is needed to perform this experiment due to its small form factor) such as its rolling shutter and inability to read its frame exposure clock prevent this method from being implemented.

Behavior Video

The behavior video was imported using the OpenCV library for Computer Vision, the videos were then decoded and saved as RAW 8-bit grayscale video files using the Numpy Python library. Finally, using the same method as described in the previous section, we removed the dark frames (prior to infrared illumination). We capture behavior video at a resolution of 320x180 pixels at 90Hz (higher time resolution to potentially track whisking) and we find that we do not drop any frames. Since the calcium imaging and behavior video have different sampling rates we use the behavioral video frames closest to the GCaMP signal in time. At the end, the synchronization of the three videos were verified by computing the total capture time in all three cameras and ensuring that they are within one calcium imaging frame time (34.7ms).

Gradient Triggered Maps

Gradient triggered maps (GTMs) were created by first selecting a region of interest (ROI) in the behavior video where luminance changes were due to a gross changes in mouse posture, whisking or paw movements. We compute the mean luminance across pixels within the ROI and then we calculate its gradient across time (Figure 2D). This results in a vector where large values correspond to points in time where the behavior (movement) was occurring. We then smooth the temporal gradient of the mean

luminance by convolving the signal with a gaussian (**σ**=20). A threshold was then established on the smoothed temporal gradient at the mean + 3 standard deviations (Figure 2D, red line). Using this threshold, the calcium imaging frames corresponding to the threshold exceeding times were extracted, and the mean across space of the selected images was computed (Figure 2 C). This ultimately results in a brain activity map that corresponds to gross behavior. For instance, an ROI placed across the whiskers of the mice will produce a gradient in which threshold crossing events indicate times where the mice were whisking (Figure 2A-E).

Whisker Stimulation

To verify the results of the whisker triggered GTMs we anaesthetized a mouse and stimulated two sets of whiskers, the macrovibrissae and the microvibrissae (Deschênes et al., 2012). The stimulation protocol consisted of 49 stimuli presented every 10 seconds, where each stimulus consisted of a one second 12 Hz sine wave, delivered with a piezoelectric vibration transducer. We then computed the $\Delta F/F_0$ for each of these extracted epochs and averaged them together across time. A similar $\Delta F/F_0$ was calculated for the shorter blue reflected light channel and was used to correct for hemodynamic signal as described earlier. This results in an average response activity video for each of the stimulation protocols. Finally, we calculated the area of peak response for the two videos and compared them.

Global Signal Analysis

We imported the two processed imaging video files into a Jupyter Notebook. Then we calculated the global signals of both mouse brain videos, which refers to an average signal of all the pixels that are considered brain. The delineation of the brain ROI was done by hand, by creating two polygons that outlined the two hemispheres of the brain. Then to calculate the global signal we take the mean of the brain pixels across time. At the end of this pipeline we obtained two vectors that corresponded to the

global signal of the left mouse and the global signal of the right mouse. Next we filtered the two global signals at ten different frequency bands: 0.01-0.1Hz, 0.1-0.5Hz, 0.5-1.0Hz, 1.0-2.0Hz, 2.0-3.0Hz, 3.0-4.0Hz, 4.0-6.0Hz, 6.0-8.0Hz, 8.0-10.0Hz, 10.0-12.0Hz. Then for each of these frequency bands we calculated a dynamic measure of signal correlation by using a sliding window and calculating the correlation coefficient between the two signals for each window of time (see supplementary video). We shifted the window one frame each time, and the size of the window is 3800 frames for the figures and 2000 frames for the video (just for viewing purposes). We chose the window size of 3800 frames because we wanted to capture a large portion of the interaction as we shifted the window.

Results

The Setup and Cross Mouse Synchronization

We have developed software and hardware which enables simultaneous acquisition of cortical functional activity (changes in intracellular calcium concentration) from two interacting GCaMP mice. The system employs relatively compact Raspberry Pi CMOS cameras allowing the two mice to be positioned within 6mm of each other (Figure 1A). The experiments were conducted by imaging mice under two conditions that were defined as together or separate. During together experiments we initially calculated regional functional connectivity using a seed based analysis using zero-lag Pearson correlation (Mohajerani et al., 2013). This procedure allowed us to examine within mouse (Supplementary Figure 1) and between mouse correlations within cortical activity (Figure 1F,G). For example, by seeding a site in one mouse we could detect correlation within networks of the other mouse. Areas which showed high levels of correlation, between mice included barrel cortex, as well as limb areas. These correlations were significantly higher than those reported for mice which were kept separated (Figure 1G).

Gradient Triggered Maps Reveal Mutual Whisking Behavior

Using the two mouse imaging paradigm, we observed mutual whisking when mice would first contact each other (see Figure 2A-E) which resembles the social touch behavior previously shown in rats (Lenschow and Brecht, 2015). To examine the relationship between mutual whisking and calcium activity, we used a gradient-triggered behavioral mapping method which examined a position in space where whiskers of the two mice would first touch (Figure 2A), then we locate the points in time where this region of space has large luminance changes, in this case the luminance changes would correspond to mice whisking. Then we find the corresponding calcium activity frames and average them, creating a map of the calcium activity that is associated with the luminance changes in the behavior video. We created a mask around the the maximally activated brain area in the averaged map and extracted the top 75% values in that mask for the originally selected calcium frames. Effectively we measured the magnitude of the cortical calcium activity changes associated with the whisking behavior. This method indicated a significant change in the GCaMP signal within the posterior barrel cortex (Figure 2C,E). We find that the area that is activated during this social touch like behavior corresponds to the macrovibrissae area of the mice (Supplementary Figure 2A,B) and not the microvibrissae area (Supplementary Figure 2C,D).

We performed the same type of mapping and magnitude of activity extraction to show that the cortical activity that emerges from mutual mouse whisking is different than activity from a lonely mouse (left mouse) whisking (obtained from the separate experiments; Fig. 2F). Additionally since we were still recording the brain activity from the right mouse in the separate experiments we are able to show that triggering from the behavior of the left mouse results in no significant calcium dynamics for the right mouse (the two mice could not interact) (Figure 2F). We find that this difference is significant across the together and separate experiments (Figure 2F).

Whisker Stimulation Reveals Similar Spatial Maps as the GTMs

To further evaluate whisker-triggered activity and its relationship to GTMs we mapped the whisker somatosensory cortex using a piezo translator to move whiskers in anaesthetized mice (Supplementary Figure 2). This mapping consistent with previous studies (Supplementary Figure 2), indicated that the longer macrovibrissae whiskers which make contact first and have a spatial profile most similar to the gradient-triggered maps (data not shown). While stimulating shorter microvibrissae whiskers led to a map located in more anterior cortical areas (Supplementary Figure 2b) as expected from previously reported functional anatomy for rodent barrel cortex.

Global Cortical Signals Synchronized at 0.01-0.1Hz Frequency Band

While evaluating gradient-triggered maps, as well as regional correlations across mice, we noticed significant correlated/coincident activity within non-whisker areas. To better evaluate brain-wide activity, we calculated global signal changes across the entire masked region of the two cortical hemispheres, see Figure 3A for a representative mouse pair example of correlated global signals. To quantify the timing at which the global signals are correlated we employed sliding window correlation and we evaluated whether the syncing of global signals occurs at specific frequency bands. When correlating the global signals of the mice across different frequency bands we find dynamic correlation specifically within the 0.01-0.1Hz band for the together experiments that starts when the mice are brought together almost until they are separated (Figure 3B). This correlation was not present for the separated experiments, and this difference was significant (Figure 3C) under the Wilcoxon rank-sum test beginning at time points when the mice are together. This non-parametric statistical hypothesis test compares two samples and assesses whether their population means are different. In our case we tested whether pairs of correlations coming from either the separate or together experiments differed at specific time-points of the experiment by sliding the test across timepoints for both groups of mice. We took each of the sample pairs, containing 14 correlation coefficients (7 separate 7 together) and ran the test, then we moved to the next time point of

the windowed correlation and re-ran the test. The population means are not significantly different at the beginning of the experiment, which is understandable since the mice are not able to interact. As the mice are brought together the difference between the means becomes significant, however the significant difference disappears before the mice are fully separated suggesting synchronization of the global signals is transient (Figure 3C).

Global Signal Synchronization Not Explained by Hemodynamics

It could be possible that the synchronization between the global signals of the two mice is in part due hemodynamic changes that indirectly affect GCaMP6 fluorescence (despite the corrections we perform, see Methods). To answer this question we performed the same type of experiments on a Thy1-GFP mice line (Feng et al., 2000). The fluorescence changes observed in this line would not reflect intracellular calcium changes in neurons, but instead would reflect hemodynamic changes (Ma et al., 2016b). We find that there is no correlation between simultaneously imaged GFP mice at all frequency bands for both separate and together experiments, as tested by the same test as the GCaMP experiments (Supplementary Figure 3, compare with Figure 3C). These experiments imply that the global signal synchronization we observe in the GCaMP6s mice is inconsistent with a hemodynamic artifact. (Deschênes et al., 2012; Feng et al., 2000). Additionally, these experiments show that the brain-wide correlations cannot be explained by external factors such as contamination of the illumination or some other hardware related factor and instead the observed correlations are indeed calcium activity changes in the two mice.

Discussion

The ability to image large expanses of the cortex while two mice interact is novel. Previous studies have examined interacting rats while acquiring electrophysiological data from cortical areas such as the barrel cortex (Bobrov et al., 2014; Ebbesen et al., 2017; Lenschow and Brecht, 2015), or have used photometry

to examine subcortical structures (Gunaydin et al., 2014). Recordings from the amygdala (Allsop et al., 2018) or hypothalamus (Füzesi et al., 2016) in the context of mesoscale cortical imaging may be informative as interacting mice perceive each other. While we assume these are social interactions, there is the possibility that fear, as well as novelty may be expressed during the mouse to mouse presentations. While these previous studies were critical for motivating our work, defining large scale interbrain synchrony was not necessarily the goal of these animal paradigms. Electrophysiological recordings (Bobrov et al., 2014; Ebbesen et al., 2017; Lenschow and Brecht, 2015), although fast temporally have limited spatial resolution (Scanziani and Häusser, 2009) and were confined to one animal limiting evaluation of inter-animal synchrony. Modulating the distance between the mice using the rail system constrains the social interaction and will allow trial averaging and future phenotyping of mouse lines to address questions regarding the genetics of social interaction in a more consistent way. Previous studies had investigators handle animals to bring them close to another rat, which may introduce some confounding factors or variability (Lenschow and Brecht, 2015). Thus, by placing the entire imaging setup inside a noise reduction box and being able to change the inter-mouse distance remotely, we were able diminish additional external confounding factors creating more standardized encounters between the two mice. A strength of this dual imaging system is the small form factor of the Raspberry Pi imaging cameras. Previously, we have employed the Dalsa 1M60 camera for our mesoscopic experiments (Harrison et al., 2009), however, this camera would not have been suitable for dual mouse imaging because of its large form factor, the camera body itself is 94x94x45mm. Placing two of these cameras next to each other would not allow the mice to come close enough for whiskers to touch. Larger cameras could employ optical relays so their physical dimensions would not be limiting.

Our results indicate surprisingly widespread synchronization of cortical activity between mice. While synchrony is clear within the current set of experiments, it was not possible to understand what the global

signal synchronization means or whether it is causally related to social interaction behaviors. It is unclear whether there is an overt behavior that correlates with the synchronization at 0.1-1 Hz (Chan et al., 2015; He et al., 2018; Mateo et al., 2017; Mitra et al., 2018; Okun et al., 2018; Winder et al., 2017), or if this reflects the ebb and flow of the whisking behavior and spread of signal out of the barrel cortex as has been observed previously (Ferezou et al., 2007; Jacobs and Frostig, 2017; Mohajerani et al., 2013). Our setup necessitates that the mice be head-restrained in order for them to be imaged and positioned properly. In a previous study head-fixation was found to be aversive, but with training and habituation stress recedes (Guo et al., 2014) and rodents can even be trained to restrain themselves (Aoki et al., 2017; Murphy et al., 2016; Scott et al., 2013). For this reason we present the results as an interaction that occurs in the context of head-fixation and caution that the observed brain dynamics may not be entirely reflective of true natural social touch behavior.

The power of mesoscale imaging in the context of social interactions is largely unexplored. For instance, we could employ more advanced computational methodology to analyze high-dimensional brain data and tease out the behavior that is associated with the global signal synchrony (Musall et al., 2018; Stringer et al., 2018). In these studies they used linear and latent factor models to discover that most of the variance in brain activity can be explained by mouse body movements and changes in pupil diameter. To further explore activity associated with this behavior the possibility of combining mesoscopic imaging with electrophysiology exists. In a similar way as a technique previously published by our laboratory (Xiao et al., 2017), in which the mice underwent cortical mesoscale imaging while signals from subcortical or cortical electrodes were recorded. Based on discrete subcortical spiking, spike triggered average cortical maps were created. Previous research has shown that activation of the dopaminergic neurons of the ventral tegmental area that project to the nucleus accumbens causally modulates social behavior in mice (Gunaydin and Deisseroth, 2014). Therefore, a follow-up experiment would be to optogenetically

stimulate the same population of cells and observe if the global brain signal synchrony still manifests with this social touch paradigm. Another follow-up experiment would be to allow imaging other types of behaviors, for example imaging the sniffing of the anogenital region which is a behavior associated with mating (Grant and Mackintosh, 1963), thus exploring whether or not there are any sex differences and not just imaging male-male interactions. Finally, exploring whether any differences exist with this social touch paradigm across different mouse strains would be very useful for understanding social disorders. For example comparing mice that exhibit autistic-like phenotypes such as the Shank3 or ProSAP1/Shank2 mutant mice (Peça et al., 2011; Schmeisser et al., 2012).

While we have employed GCAMP6 imaging of genetically targeted indicators of intracellular calcium, the dual mouse imaging paradigm may be an ideal place to examine lower frequency events that are revealed using fNIRs or intrinsic optical signals (Montague et al., 2002; Funane et al., 2011; Yücel et al., 2017; Liu et al., 2017). Although restricted to cortical signals, the non-invasive nature of activity measurements based on differential light absorbance (Strangman et al., 2002) which correlate with fMRI signals are a significant advantage for human studies. Given these signals are of lower temporal resolution than GCAMP6, they are well positioned to sample transients below 0.1 Hz. The use of fNIRs in animals may aid the development of human brain imaging sequences and analysis routines that leverage inter-subject interactions.

Overall we suggest that the power of the dual mouse mesoscale imaging platform will be in creating a reproducible interaction between mice that may constrain some of the possible behaviors and timing due to staging we impose through the rail-based system. Such constraint may be particularly important when evaluating the behavior of different mouse mutants associated with disorder of social interactions.

Figure legends.

Figure. 1 Setup for dual mouse brain imaging and inter-mouse brain correlation. A) Cartoon showing epifluorescence imaging system for dual mouse experiments. The system employs a Raspberry Pi Camera with an RGB CMOS sensor. A triple band emission filter was used to parse green epifluorescence signals associated with GCaMP6s from a shorter blue reflected light signal used for hemodynamic correction. These signals fall onto green and blue channels respectively of the RGB sensor. Fluorescence and reflection illumination was performed using liquid light guide positioned over the mouse of interest and care is taken to avoid directly illuminating the eyes. A rail system was used to vary the distance between the snouts of the mice from 6mm up to 160mm. B) Transcranial window used for intact skull mesoscale imaging. Cartoon showing approximate location of titanium head fixation bar and custom cut coverslip. C) Cartoon of the modified coverslip that was used to cover the mouse's skull next to a cartoon of the mouse brain to get an estimate of size covered. D) Dimensions of the titanium bar that was glued to the skull of the mouse. E) Dual mouse fluorescence imaging rigs build around Sherline Tools vertical milling machine stand and Thorlab parts. Note: the system is movable using an Edmunds optics 25 cm linear translator (56-798) which is connected to a flexible-shaft remote control (McMaster Carr 6426K62). F) Calcium signals from 11 brain areas (based on stereotaxic coordinates with respect to bregma) were parsed out for the points in time of the experiment where the mice were together (6-12mm apart) a total of 135s. The signals from the left mouse were correlated against the signals of the right mouse for all the regions of interest, the zero-lag Pearson correlation coefficient is displayed on the matrix (the calibration is in units of correlation). The 11 brain regions have the following abbreviations: AC anterior cingulate; aBC, Barrel Cortex anterior; pBC, Barrel Cortex posterior; FL, forelimb; and HL, hindlimb regions of the primary somatosensory area; RS, retrosplenial area; mPTA medial parietal association area; lPTA lateral parietal association area; V1 primary visual area; M1, primary motor area; and Un, unassigned multimodal region.

G) The same procedure was was performed on the separate experiments, taking the same time points as above (135s), however the mice were never brought to within interacting distance. Calcium signals from the same 11 brain areas were correlated between the two mice.

Figure 2. Gradient-triggered maps and activation within posterior barrel cortex during mouse interaction. A) Still video image of mice in the together experimental mode (snouts 6-12mm apart), along with the ROI that was selected to detect when the mice are whisking. B) Brain cartoon with regions of interest where cortical imaging was performed. C) Gradient-triggered maps (averaged calcium frames) triggered on points in time of the behavior video where the selected ROI in A showed large changes. The selected calcium frames were averaged and a map associated with the points in time where the mice are whisking emerges. The two arrows highlight the areas where the signals in E are plotted from, the posterior barrel cortex. The blue curve is for the left mouse and the red curve is for the right mouse. D) Plots of the smoothed gradient extracted from the region of interest in A. The mice start out 160mm away from each other and then were brought together (green shaded region), the gradient at that point becomes larger because the mice begin whisking. The mice begin moving at 90s (at around 105s they were together), then at 240s the mice were moved apart. E) GCaMP fluorescence corrected by short blue light reflection extracted from hand-drawn polygons from the areas with arrows pointing to them in C. When the whisker gradient in D has large changes the brain calcium signals were also changing. F) From the non-averaged calcium imaging frames that created the maps in C and the polygons drawn on the posterior barrel cortices we extracted the 75th percentile of the values inside the mask to compare between groups: this was done for each of the together experiments, separate experiments. Within the separate experiments we made a distinction between separate triggered and separate untriggered. Separate triggered means that the left mouse was the one that was capable of making the luminance gradient large, and separate untriggered refers to the brain signals read from the right mouse (where no behavioral camera was

present), as this mouse was not capable of influencing the gradient since it was far away from the left mouse.

Figure 3. Global signal synchronization during mouse interaction. A) Plots of global signal activity (the average of all areas within the masked hemispheres) showing synchronization in the green shaded area when the mice were brought together for a representative example GCaMP6s mouse pair. B) Average frequency spectrogram of the sliding window correlations during separate and together experiments (n=7 pairs). A prominent band is observed in the low infraslow frequency range indicating infraslow activity synchronization. The dotted white lines indicate the period where the mice were together. The start and end times are different for panels B and C since data at the beginning and end of the record were not used because of limitations in the analysis procedures (sliding window time). C) Statistical testing of group data for global signal correlation values between separate and together experiments (7 pairs) in the 0.01-0.1 Hz frequency using the Wilcoxon rank-sum test across the indicated time points. The dotted black lines indicate when the mice were together.

Supplementary Figure 1. Correlation maps intra-brain group data. A) Similar analysis as in Figure 1F,G, however the signals of the 11 brain areas were correlated against intra-brain values (rather than between mouse) in the together experiments, n=7 for each of the matrices left and right mice. B) Same analysis as A, however these matrices are from the separate experiments, n=7 for each matrix for left and right mice.

Supplementary Figure 2. Stimulation of the micro and macrovibrissae.

A) Schematic of the location of whisker stimulation, the macrovibrissae. For stimuli we used a one second 12Hz sine wave delivered by a piezoelectric vibration transducer. B) Montage of average calcium activity for all trials. The peak activity map on frame +25 was in a similar location as the whisking GTM

found in mouse together experiments. C) Schematic of the location of whisker stimulation, the microvibrissae. For stimuli we used a one second 12 Hz sine wave delivered by a piezoelectric vibration transducer. D) Collage of average calcium activity for all trials. Notice the peak area of activation is located more anterior than the macrovibrissae area.

Supplementary Figure 3. Thy1-GFP Mice do not Exhibit Global Signal Synchronization. A) A matrix that shows the sliding window correlation at different frequency bands for the Thy1-GFP experiments. The same type of experiments as the GCaMP6s ones were performed. The matrix on the left is for the separate experiments and the right matrix shows the together experiments. There does not seem to be global signal synchronization in the GFP line. B) Global signal syncing was not significantly different between the together and separate experiments as tested by the same statistical method as the GCaMP6s experiments.

Video 1 . Sliding window correlation and global signal response for interacting mice. Shown are 2 male Thy-1 GCaMP6s mice head-fixed and undergoing the full social touch experiment. Times are in frames (28.815 frames/s, playback at 30Hz). The two pseudo-colored images show the processed calcium images from the left mouse (top) and right mouse (bottom) over the 8mm field of view of the dorsal cortex. The colorbar indicates the $\Delta F/F_0$ of the signals. The top plot on the right shows the global signals filtered at the frequency band of 0.01-0.1Hz for the left mouse (blue) and the right mouse (red). The shaded green region indicates the current window location that is used to compute the zero lag Pearson correlation between the two global signals. The bottom plot displays the current correlation between the two global signals for that particular window. The bottom video shows the behavior video for the experiment. High inter-brain correlation is observed for periods when the mice are close to one another.

References

Allen WE, Kauvar IV, Chen MZ, Richman EB, Yang SJ, Chan K, Gradinaru V, Deverman BE, Luo L, Deisseroth K. 2017. Global Representations of Goal-Directed Behavior in Distinct Cell Types of Mouse Neocortex. *Neuron* **94**:891–907.e6.

Allsop SA, Wichmann R, Mills F, Burgos-Robles A, Chang C-J, Felix-Ortiz AC, Vienne A, Beyeler A, Izadmehr EM, Glober G, Cum MI, Stergiadou J, Anandalingam KK, Farris K, Namburi P, Leppla CA, Weddington JC, Nieh EH, Smith AC, Ba D, Brown EN, Tye KM. 2018. Corticoamygdala Transfer of Socially Derived Information Gates Observational Learning. *Cell* **173**:1329–1342.e18.

Aoki R, Tsubota T, Goya Y, Benucci A. 2017. An automated platform for high-throughput mouse behavior and physiology with voluntary head-fixation. *Nat Commun* **8**:1196.

Bobrov E, Wolfe J, Rao RP, Brecht M. 2014. The representation of social facial touch in rat barrel cortex. *Curr Biol* **24**:109–115.

Brecht M, Freiwald WA. 2012. The many facets of facial interactions in mammals. *Curr Opin Neurobiol* **22**:259–266.

Chan AW, Mohajerani MH, LeDue JM, Wang YT, Murphy TH. 2015. Mesoscale infraslow spontaneous membrane potential fluctuations recapitulate high-frequency activity cortical motifs. *Nat Commun* **6**:7738.

Chen JL, Carta S, Soldado-Magraner J, Schneider BL, Helmchen F. 2013. Behaviour-dependent recruitment of long-range projection neurons in somatosensory cortex. *Nature* **499**:336–340.

Chen T-W, Wardill TJ, Sun Y, Pulver SR, Renninger SL, Baohan A, Schreiter ER, Kerr RA, Orger MB, Jayaraman V, Looger LL, Svoboda K, Kim DS. 2013. Ultrasensitive fluorescent proteins for imaging neuronal activity. *Nature* **499**:295–300.

Dana H, Chen T-W, Hu A, Shields BC, Guo C, Looger LL, Kim DS, Svoboda K. 2014. Thy1-GCaMP6 transgenic mice for neuronal population imaging in vivo. *PLoS One* **9**:e108697.

Deschênes M, Moore J, Kleinfeld D. 2012. Sniffing and whisking in rodents. *Curr Opin Neurobiol* **22**:243–250.

Ebbesen CL, Doron G, Lenschow C, Brecht M. 2017. Vibrissa motor cortex activity suppresses contralateral whisking behavior. *Nat Neurosci* **20**:82–89.

Feng G, Mellor RH, Bernstein M, Keller-Peck C, Nguyen QT, Wallace M, Nerbonne JM, Lichtman JW, Sanes JR. 2000. Imaging neuronal subsets in transgenic mice expressing multiple spectral variants of GFP. *Neuron* **28**:41–51.

Ferezou I, Haiss F, Gentet LJ, Aronoff R, Weber B, Petersen CCH. 2007. Spatiotemporal dynamics of cortical sensorimotor integration in behaving mice. *Neuron* **56**:907–923.

Funane T, Kiguchi M, Atsumori H, Sato H, Kubota K, Koizumi H. 2011. Synchronous activity of two people's prefrontal cortices during a cooperative task measured by simultaneous near-infrared spectroscopy. *J Biomed Opt* **16**:077011.

Füzesi T, Daviu N, Wamsteeker Cusulin JI, Bonin RP, Bains JS. 2016. Hypothalamic CRH neurons orchestrate complex behaviours after stress. *Nat Commun* **7**:11937.

Gilad A, Gallero-Salas Y, Groos D, Helmchen F. 2018. Behavioral Strategy Determines Frontal or Posterior Location of Short-Term Memory in Neocortex. *Neuron* **99**:814–828.e7.

Grant EC, Mackintosh JH. 1963. A Comparison of the Social Postures of Some Common Laboratory Rodents. *Behaviour* **21**:246–259.

Gunaydin LA, Deisseroth K. 2014. Dopaminergic Dynamics Contributing to Social Behavior. *Cold Spring Harb Symp Quant Biol* **79**:221–227.

Gunaydin LA, Grosenick L, Finkelstein JC, Kauvar IV, Fenno LE, Adhikari A, Lammel S, Mirzabekov JJ, Airan RD, Zalocusky KA, Tye KM, Anikeeva P, Malenka RC, Deisseroth K. 2014. Natural

neural projection dynamics underlying social behavior. *Cell* **157**:1535–1551.
Guo ZV, Li N, Huber D, Ophir E, Gutnisky D, Ting JT, Feng G, Svoboda K. 2014. Flow of cortical activity underlying a tactile decision in mice. *Neuron* **81**:179–194.
Harrison TC, Sigler A, Murphy TH. 2009. Simple and cost-effective hardware and software for functional brain mapping using intrinsic optical signal imaging. *J Neurosci Methods* **182**:211–218.
He Y, Wang M, Chen X, Pohmann R, Polimeni JR, Scheffler K, Rosen BR, Kleinfeld D, Yu X. 2018. Ultra-Slow Single-Vessel BOLD and CBV-Based fMRI Spatiotemporal Dynamics and Their Correlation with Neuronal Intracellular Calcium Signals. *Neuron* **97**:925–939.e5.
Jacobs NS, Frostig RD. 2017. Prominent lateral spread of imaged evoked activity beyond cortical columns in barrel cortex provides foundation for coding whisker identity. *Neurophotonics* **4**:031218.
Kluyver T, Ragan-Kelley B, Pérez F, Granger BE, Bussonnier M, Frederic J, Kelley K, Hamrick JB, Grout J, Corlay S, Others. 2016. Jupyter Notebooks-a publishing format for reproducible computational workflowsELPUB. pp. 87–90.
Lenschow C, Brecht M. 2015. Barrel cortex membrane potential dynamics in social touch. *Neuron* **85**:718–725.
Liu Y, Piazza EA, Simony E, Shewokis PA, Onaral B, Hasson U, Ayaz H. 2017. Measuring speaker–listener neural coupling with functional near infrared spectroscopy. *Sci Rep* **7**:43293.
Mateo C, Knutsen PM, Tsai PS, Shih AY, Kleinfeld D. 2017. Entrainment of Arteriole Vasomotor Fluctuations by Neural Activity Is a Basis of Blood-Oxygenation-Level-Dependent "Resting-State" Connectivity. *Neuron* **96**:936–948.e3.
Ma Y, Shaik MA, Kim SH, Kozberg MG, Thibodeaux DN, Zhao HT, Yu H, Hillman EMC. 2016a. Wide-field optical mapping of neural activity and brain haemodynamics: considerations and novel approaches. *Philos Trans R Soc Lond B Biol Sci* **371**. doi:10.1098/rstb.2015.0360
Ma Y, Shaik MA, Kozberg MG, Kim SH, Portes JP, Timerman D, Hillman EMC. 2016b. Resting-state hemodynamics are spatiotemporally coupled to synchronized and symmetric neural activity in excitatory neurons. *Proc Natl Acad Sci U S A* **113**:E8463–E8471.
Mitra A, Kraft A, Wright P, Acland B, Snyder AZ, Rosenthal Z, Czerniewski L, Bauer A, Snyder L, Culver J, Lee J-M, Raichle ME. 2018. Spontaneous Infra-slow Brain Activity Has Unique Spatiotemporal Dynamics and Laminar Structure. *Neuron* **98**:297–305.e6.
Mohajerani MH, Chan AW, Mohsenvand M, LeDue J, Liu R, McVea DA, Boyd JD, Wang YT, Reimers M, Murphy TH. 2013. Spontaneous cortical activity alternates between motifs defined by regional axonal projections. *Nat Neurosci* **16**:1426–1435.
Montague PR, Berns GS, Cohen JD, McClure SM, Pagnoni G, Dhamala M, Wiest MC, Karpov I, King RD, Apple N, Fisher RE. 2002. Hyperscanning: simultaneous fMRI during linked social interactions. *Neuroimage* **16**:1159–1164.
Murphy TH, Boyd JD, Bolaños F, Vanni MP, Silasi G, Haupt D, LeDue JM. 2016. High-throughput automated home-cage mesoscopic functional imaging of mouse cortex. *Nat Commun* **7**:11611.
Musall S, Kaufman MT, Gluf S, Churchland AK. 2018. Movement-related activity dominates cortex during sensory-guided decision making. *bioRxiv*. doi:10.1101/308288
O'Connor DH, Peron SP, Huber D, Svoboda K. 2010. Neural activity in barrel cortex underlying vibrissa-based object localization in mice. *Neuron* **67**:1048–1061.
Okun M, Steinmetz NA, Lak A, Dervinis M, Harris KD. 2018. Distinct structure of cortical population activity on fast and infraslow timescales. doi:10.1101/395251
Peça J, Feliciano C, Ting JT, Wang W, Wells MF, Venkatraman TN, Lascola CD, Fu Z, Feng G. 2011. Shank3 mutant mice display autistic-like behaviours and striatal dysfunction. *Nature* **472**:437–442.
Scanziani M, Häusser M. 2009. Electrophysiology in the age of light. *Nature* **461**:930–939.
Schmeisser MJ, Ey E, Wegener S, Bockmann J, Stempel AV, Kuebler A, Janssen A-L, Udvardi PT, Shiban E, Spilker C, Balschun D, Skryabin BV, Dieck ST, Smalla K-H, Montag D, Leblond CS,

Faure P, Torquet N, Le Sourd A-M, Toro R, Grabrucker AM, Shoichet SA, Schmitz D, Kreutz MR, Bourgeron T, Gundelfinger ED, Boeckers TM. 2012. Autistic-like behaviours and hyperactivity in mice lacking ProSAP1/Shank2. *Nature* **486**:256–260.

Scott BB, Brody CD, Tank DW. 2013. Cellular resolution functional imaging in behaving rats using voluntary head restraint. *Neuron* **80**:371–384.

Silasi G, Xiao D, Vanni MP, Chen ACN, Murphy TH. 2016. Intact skull chronic windows for mesoscopic wide-field imaging in awake mice. *J Neurosci Methods* **267**:141–149.

Strangman G, Culver JP, Thompson JH, Boas DA. 2002. A quantitative comparison of simultaneous BOLD fMRI and NIRS recordings during functional brain activation. *Neuroimage* **17**:719–731.

Stringer C, Pachitariu M, Steinmetz N, Reddy CB, Carandini M, Harris KD. 2018. Spontaneous behaviors drive multidimensional, brain-wide population activity. *bioRxiv*. doi:10.1101/306019

Vanni MP, Murphy TH. 2014. Mesoscale transcranial spontaneous activity mapping in GCaMP3 transgenic mice reveals extensive reciprocal connections between areas of somatomotor cortex. *J Neurosci* **34**:15931–15946.

Wekselblatt JB, Flister ED, Piscopo DM, Niell CM. 2016. Large-scale imaging of cortical dynamics during sensory perception and behavior. *J Neurophysiol* **115**:2852–2866.

Winder AT, Echagarruga C, Zhang Q, Drew PJ. 2017. Weak correlations between hemodynamic signals and ongoing neural activity during the resting state. *Nat Neurosci* **20**:1761–1769.

Xiao D, Vanni MP, Mitelut CC, Chan AW, LeDue JM, Xie Y, Chen AC, Swindale NV, Murphy TH. 2017. Mapping cortical mesoscopic networks of single spiking cortical or sub-cortical neurons. *Elife* **6**. doi:10.7554/eLife.19976

Yücel MA, Selb JJ, Huppert TJ, Franceschini MA, Boas DA. 2017. Functional Near Infrared Spectroscopy: Enabling Routine Functional Brain Imaging. *Curr Opin Biomed Eng* **4**:78–86.

Zhuang J, Ng L, Williams D, Valley M, Li Y, Garrett M, Waters J. 2017. An extended retinotopic map of mouse cortex. doi:10.7554/eLife.18372

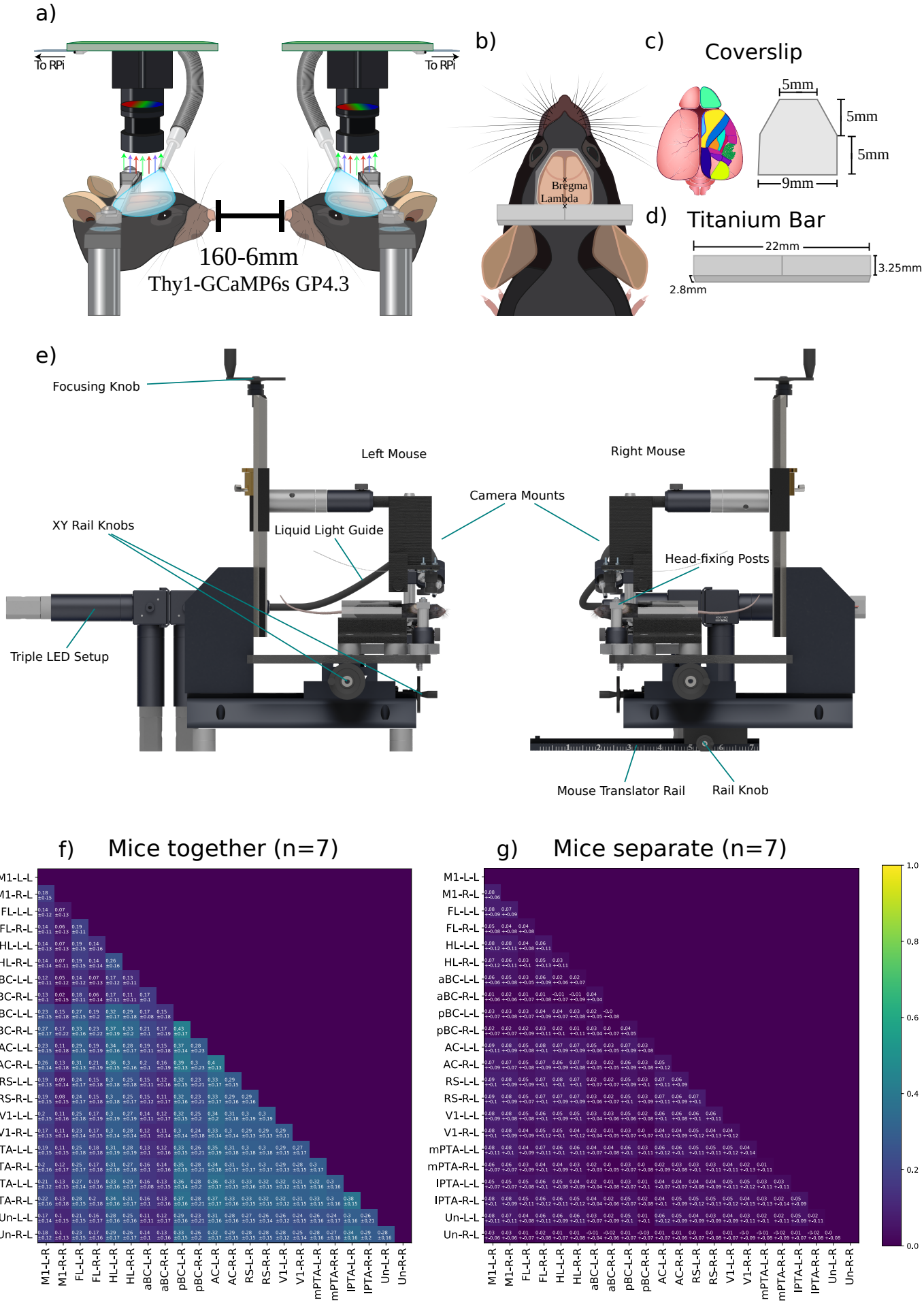
a)
To RPi
To RPi
160-6mm
Thy1-GCaMP6s GP4.3
b)
Bregma
Lambda
c)
Coverslip
5mm
5mm
5mm
9mm
d)
Titanium Bar
22mm
3.25mm
2.8mm
e)
Focusing Knob
Left Mouse
Right Mouse
Camera Mounts
XY Rail Knobs
Liquid Light Guide
Head-fixing Posts
Triple LED Setup
Mouse Translator Rail
Rail Knob
f)
Mice together (n=7)
g)
Mice separate (n=7)
M1-L-L
M1-R-L
FL-L-L
FL-R-L
HL-L-L
HL-R-L
aBC-L-L
aBC-R-L
pBC-L-L
pBC-R-L
AC-L-L
AC-R-L
RS-L-L
RS-R-L
V1-L-L
V1-R-L
mPTA-L-L
mPTA-R-L
IPTA-L-L
IPTA-R-L
Un-L-L
Un-R-L
1.0
0.8
0.6
0.4
0.2
0.0

Figure 1

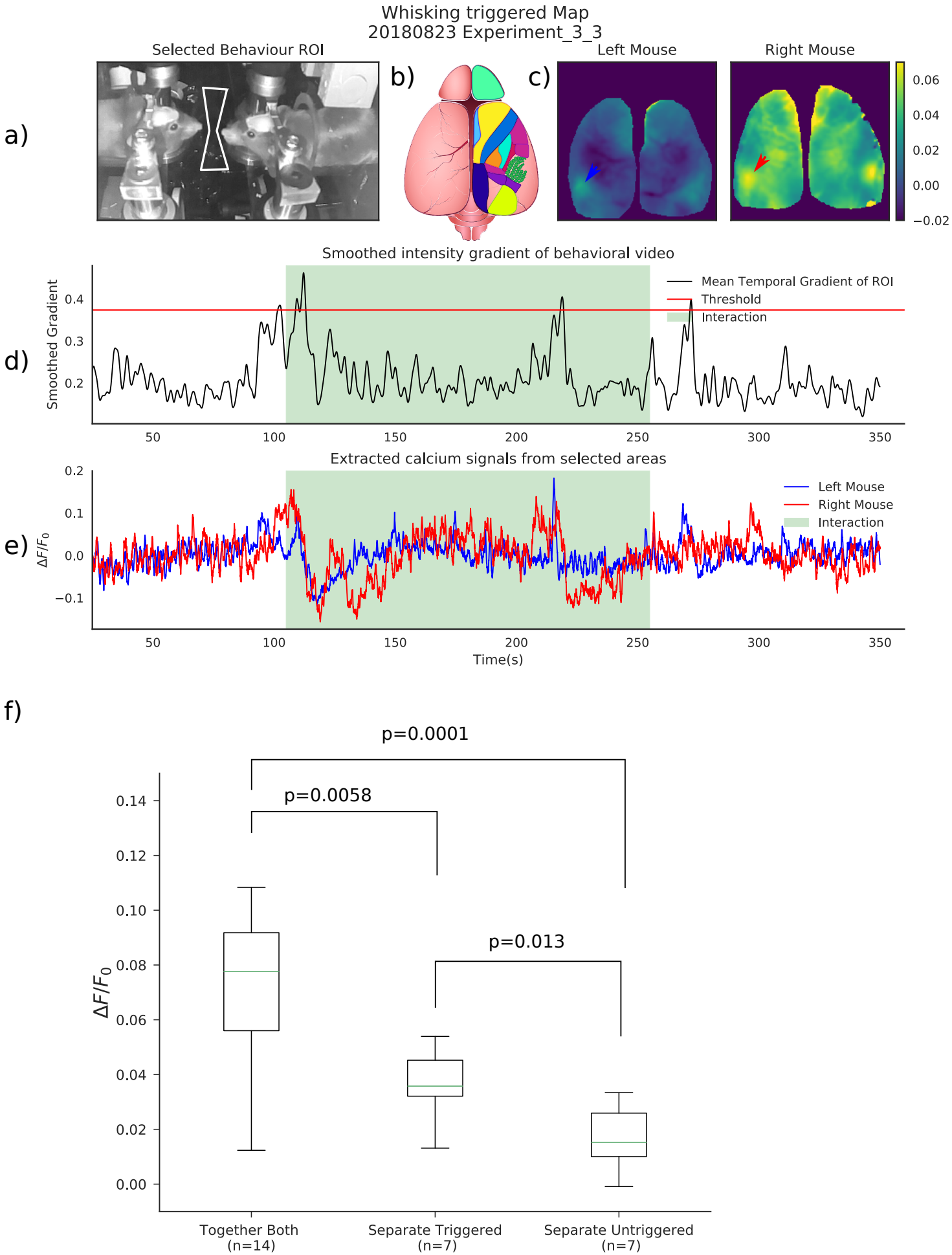
Whisking triggered Map
20180823 Experiment_3_3
a)
Selected Behaviour ROI
b)
c)
Left Mouse
Right Mouse
0.06
0.04
0.02
0.00
−0.02
d)
Smoothed intensity gradient of behavioral video
Smoothed Gradient
Mean Temporal Gradient of ROI
Threshold
Interaction
e)
Extracted calcium signals from selected areas
ΔF/F0
Left Mouse
Right Mouse
Interaction
Time(s)
f)
p=0.0001
p=0.0058
p=0.013
ΔF/F0
Together Both (n=14)
Separate Triggered (n=7)
Separate Untriggered (n=7)

Figure 2

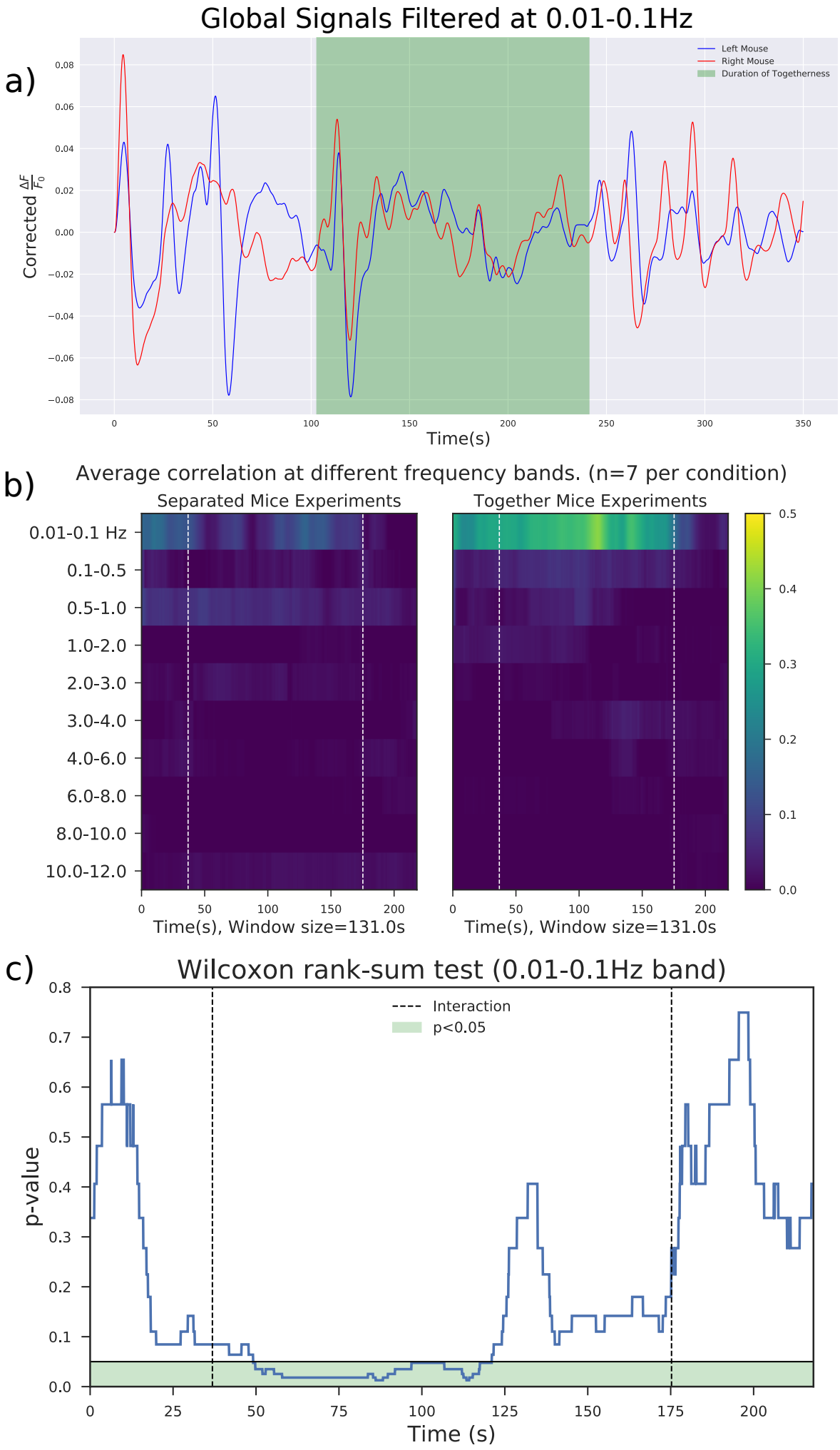
Global Signals Filtered at 0.01-0.1Hz
a)
Left Mouse
Right Mouse
Duration of Togetherness
Corrected $\frac{\Delta F}{F_0}$
Time(s)
b)
Average correlation at different frequency bands. (n=7 per condition)
Separated Mice Experiments
Together Mice Experiments
0.01-0.1 Hz
0.1-0.5
0.5-1.0
1.0-2.0
2.0-3.0
3.0-4.0
4.0-6.0
6.0-8.0
8.0-10.0
10.0-12.0
Time(s), Window size=131.0s
Time(s), Window size=131.0s
c)
Wilcoxon rank-sum test (0.01-0.1Hz band)
Interaction
p<0.05
p-value
Time (s)

Figure 3